Integrated Cycle and Turbomachinery Design of an Intercooled Helium Brayton Cycle for HTGR

Byung Chul Kim [a], Jeong Ik Lee [a*]
[a]*Dept. of Nuclear & Quantum Eng., KAIST,* 291 Daehak-ro, Yuseong-Gu, Daejeon 34141, Republic of Korea
[a*]*Corresponding author: jeongiklee@kaist.ac.kr*

***Keywords : Helium Brayton cycle, HTGR, Turbomachinery design, Cycle optimization**

1. Introduction

High Temperature Gas-cooled Reactors (HTGR) use helium as the coolant and can reach high outlet temperatures, enabling direct coupling with a Brayton-cycle power conversion system; a direct helium Brayton cycle has therefore been studied as a leading option for small modular HTGRs [1]. Ahn et al. showed that intercooling reduces compression work and improves efficiency in a recuperated helium Brayton cycle for a small HTGR [1].

Turbomachinery performance is an especially important driver of overall cycle performance for smaller HTGRs, where reduced flow rates and cycle scale place tighter constraints on machine design. Bae et al. compared intercooling configurations for a 20 MW_{th} HTGR and showed, via ns-ds diagram-based preliminary sizing, a trade-off between high pressure (favorable for smaller turbomachinery) and the higher rotational speed it requires [2]. The same underlying sensitivity also appears on a larger scale. Direct-cycle programs such as the GT-MHR have had to evaluate multiple helium power-conversion-unit configurations at the several-hundred-MW_{th} level [3]. Operating experience from helium gas-turbine plants and test facilities shows that helium's low molecular weight — which demands higher rotational speeds and stage count than air- or CO2-based machines — makes turbomachinery design an unusually influential factor across the whole range of HTGR power ratings [4].

This prior study assumed fixed turbine/compressor isentropic efficiencies during cycle optimization and evaluated turbomachinery size only afterward, even though actual efficiency depends on mass flow, pressure ratio, speed, stage number, and geometry [2]. Because compressor power is large relative to turbine output in helium cycles, a mismatch between assumed and actual efficiency can shift not only net power but the optimal pressure ratio itself. A similar cycle–turbomachinery coupling has been explored for supercritical CO2 cycles [5].

This study closes that gap for a 90 MW_{th} HTGR with a single-intercooled recuperated direct helium Brayton cycle. A REFPROP-based Closed Cycle Design (CCD) first finds the thermodynamic optimum over the total compressor pressure ratio and the LP/HP pressure-ratio split. The resulting conditions are then used to size the LP and HP compressors and the turbine, first through ns-ds diagram preliminary sizing (TMSK) and then through detailed loss-model turbomachinery design (TMD). Finally, the TMD derived efficiencies are fed back into the CCD model to re-optimize the cycle, quantifying the shift between the two optima.

2. Analysis Method

2.1 System Configuration and Boundary Conditions

This study analyzes a single-intercooled recuperated direct helium Brayton cycle coupled to a 90 MW_{th} HTGR. As shown in Fig. 1, the cycle comprises the HTGR, turbine, recuperator, precooler, LP compressor, intercooler, and HP compressor: helium heated in the reactor expands through the turbine, is cooled on the recuperator hot side and in the precooler, is compressed in two stages (LP compressor, intercooler, HP compressor), reheated on the recuperator cold side, and returned to the reactor. This single-intercooling layout has been shown to reduce compression work and improve efficiency in prior small-HTGR helium Brayton cycle studies [1,2].

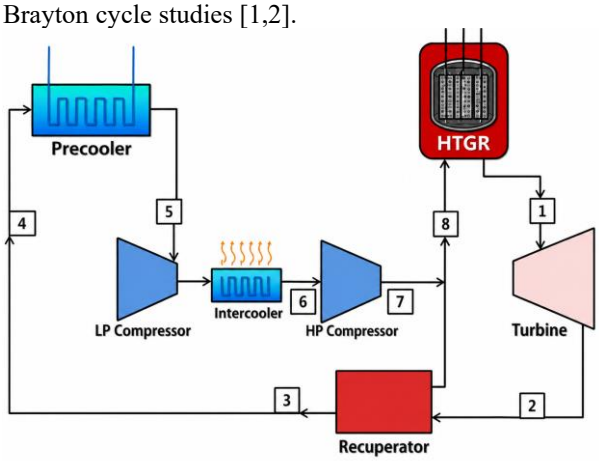


Fig. 1. Schematic of the single-intercooled recuperated direct helium Brayton cycle

Reactor thermal power was fixed at 90 MW_{th}, with a reactor outlet temperature of 750°C and a minimum cycle temperature of 35°C. The reference pressure on the high-pressure side of the cycle — state 7, the HP compressor outlet, which sets the numerator of the total compressor pressure ratio defined in Section 2.2 — was fixed at 7 MPa, consistent with the helium pressure levels used in [1,2]. This value was held constant while the total compressor pressure ratio was swept, so it functions as a fixed upper-pressure anchor rather than an independently optimized reactor pressure; the low-

pressure-side state (state 4) varies accordingly with the swept pressure ratio, which is the primary optimization variable in this study.

The initial CCD assumed a turbine isentropic efficiency of 0.88 and LP and HP compressor isentropic efficiencies of 0.80, together with a recuperator effectiveness of 0.95, as summarized in Table 1; these values serve only as initial design assumptions and are later replaced by TMD-predicted efficiencies in Section 2.4. A pressure drop of 100 kPa was assumed across the reactor, 60 kPa on the recuperator hot side and 30 kPa on the cold side, and 20 kPa each across the precooler and intercooler, all adopted from [2]. The intercooler outlet temperature was fixed at 35°C, matching the precooler outlet, so that the LP and HP compressors operate under comparable inlet-temperature conditions. These conditions form the basis for the CCD optimization, the TMSK/TMD turbomachinery design, and the TMD-informed re-optimization described in the following sections.

Table 1. Main boundary conditions and initial assumptions for CCD analysis

Parameter	Value
Reactor thermal power	90 MW_{th}
Reactor outlet temperature	750°C
Minimum cycle temperature	35°C
High-pressure reference pressure	7 MPa
Working fluid	Helium
Cycle configuration	Direct, recuperated, single intercooling
Turbine isentropic efficiency	0.88
LP compressor isentropic efficiency	0.80
HP compressor isentropic efficiency	0.80
Recuperator effectiveness	0.95

2.2 Thermodynamic Cycle Optimization

The thermodynamic optimum of the helium Brayton cycle was obtained from a steady-state energy-balance-based CCD, with helium properties (enthalpy, entropy, density) evaluated using REFPROP 10.0 [6]. State points follow Fig. 1: 1 = reactor outlet/turbine inlet, 2 = turbine outlet, 3 = recuperator hot-side outlet, 4 = precooler outlet, 5 = LP compressor outlet, 6 = intercooler outlet, 7 = HP compressor outlet, 8 = recuperator cold-side outlet.

The turbine and compressors were modeled as adiabatic with isentropic efficiency:

$$h_{out} = h_{in} + \frac{h_{out,s} - h_{in}}{\eta_c} \quad (1)$$

$$h_{out} = h_{in} - \eta_t(h_{in} - h_{out,s}) \quad (2)$$

where $h_{out,s}$ is the isentropic outlet enthalpy at the actual outlet pressure. The recuperator was modeled as a counterflow exchanger with equal mass flow on both sides; the maximum recoverable heat was set by the hot- and cold-side enthalpy difference, and the actual duty was obtained by applying the effectiveness in Table 1. To avoid a non-physical internal temperature cross, the recuperator was discretized into 41 nodes, and only cases with a minimum internal $\Delta T \geq 10$ K were retained as feasible.

The two optimization variables were the total compressor pressure ratio,

$$PR_{tot} = \frac{P_7}{P_4} \quad (3)$$

and the LP/HP pressure-ratio split, expressed through

$$PR_{LP} = \frac{P_5}{P_4}, \qquad PR_{HP} = \frac{P_7}{P_6} \quad (4)$$

and a pressure-ratio bias

$$B_{PR} = \frac{PR_{LP}}{PR_{HP}} \quad (5)$$

where B = 1 denotes an equal split and B ≠ 1 biases the pressure rise toward the HP or LP compressor. PR_{tot} was swept over 1.15–4.00 (116 points) and B over 0.70–1.30 (61 points), giving 7,076 design points. At each point the required mass flow followed from the fixed reactor duty,

$$\dot{m} = \frac{Q_{HTGR}}{h_1 - h_8} \quad (6)$$

where h_8 denotes the reactor inlet enthalpy (state 8, the recuperator cold-side outlet), and net power and thermal efficiency were

$$W_{net} = W_T - W_{LPC} - W_{HPC} \quad (7)$$

$$\eta_{th} = \frac{W_{net}}{Q_{HTGR}} \quad (8)$$

Fig. 2 summarizes the sweep results. Fig. 2(a) shows thermal efficiency versus total compressor pressure ratio for the equal-split (B = 1) and pressure-ratio-optimized cases: both curves nearly coincide, and the maximum efficiency, η_{th} = 39.63% at PR_{tot} = 1.869, is essentially unaffected by the LP/HP split. Fig. 2(b) shows the corresponding optimized LP and HP compressor pressure ratios and the net specific work as functions of PR_tot; at the optimum, PR_{LP} = 1.342 and PR_{HP} = 1.398 — a nearly equal split — while net specific work increases monotonically with PR_{tot}. Together, the two panels indicate that at this operating point the total pressure ratio, rather than the LP/HP split, is the dominant driver of cycle efficiency, consistent with compression work being minimized when the two stages operate under similar inlet-temperature conditions [1,2]. The resulting optimum gives a net power of 35.67 MW and a helium mass flow of 82.14 kg/s.

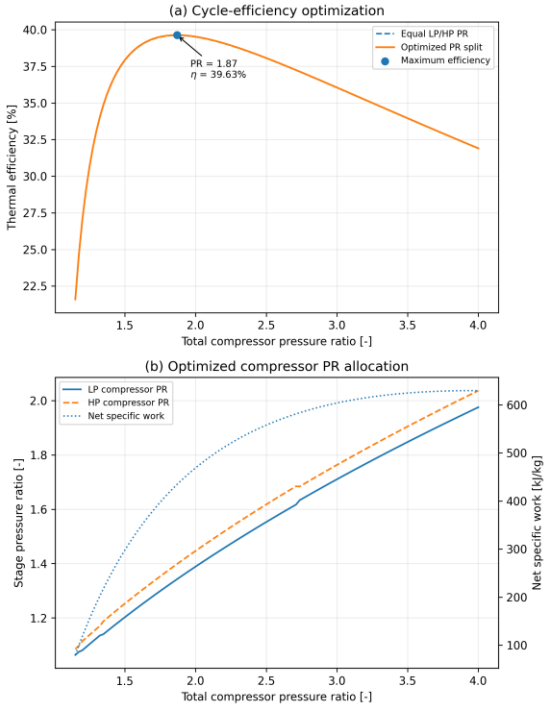


Fig. 2. Thermodynamic optimization of the intercooled helium Brayton cycle: (a) thermal efficiency with total compressor pressure ratio and (b) optimized LP/HP compressor pressure-ratio allocation and net specific work.

2.3 Turbomachinery Design

Using the mass flow, and inlet/outlet pressures and temperatures from the CCD optimum, the LP compressor, HP compressor, and turbine were designed in two stages: a preliminary sizing (TMSK) followed by a detailed mean-line design (TMD). TMSK uses Balje's specific speed–specific diameter ($n_s - d_s$) diagram [7] to estimate stage efficiency and characteristic diameter as a function of rotational speed and stage number. The specific speed is computed directly from the known angular speed, volumetric flow rate, and adiabatic head:

$$n_s = \frac{\omega\sqrt{\dot{V}}}{(gH_{ad})^{3/4}}, \qquad d_s = \frac{D(gH_{ad})^{1/4}}{\sqrt{\dot{V}}} \tag{9}$$

where ω is angular speed, $\dot{V}$ is volumetric flow rate, H_{ad} is adiabatic head, and D is characteristic diameter. For each computed ns, the specific diameter ds are read from the diagram along the highest-efficiency locus, and Eq. (9) is then rearranged to solve for D. Following [2], a maximum tip speed of 500 m/s was applied as a feasibility limit.

TMSK screened both radial and axial topologies over a common shaft speed of 6,000–36,000 rpm, with 1–6 compressor stages and 1–10 turbine stages; a case was feasible if every stage's ns fell within the diagram range and tip speed stayed within the 500 m/s limit. Among the feasible cases, screening selected a radial configuration at 8,000 rpm, with 2, 3, and 5 stages for the LP compressor, HP compressor, and turbine, respectively, giving preliminary isentropic efficiencies of 81.70%, 82.16%, and 90.15%. The radial configuration outperformed the axial alternatives across the screened range, consistent with the low specific speed characteristic of small-scale, high-rotational-speed helium turbomachinery, where axial designs require long, narrow blade passages that incur higher viscous losses than radial designs [7].

These conditions were then carried into a detailed 1-D mean-line TMD for the radial machines. Compressor losses included incidence, blade loading, skin friction, clearance, disk friction, mixing, recirculation, and leakage; turbine losses included incidence, rotor-passage, clearance, and disk friction. A compact geometry search (axial velocity, vane number, compressor back sweep angle, and diameter ratios) selected the highest-efficiency design meeting the tip-speed limit; only on-design performance was evaluated.

Fig. 3(a) compares TMSK and TMD efficiencies: the detailed TMD gives an LP compressor isentropic efficiency of 89.94%, an HP compressor efficiency of 89.38%, and a turbine efficiency of 93.86%, all higher than the TMSK estimates and the values assumed in the initial CCD, where the LP and HP compressor efficiencies were set to 80% and the turbine efficiency to 88%. The maximum characteristic diameter reached 1.77 m for the LP compressor, 1.54 m for the HP compressor, and 1.72 m for the turbine, and the turbine's maximum tip speed reached 498.9 m/s, close to the 500 m/s limit. Fig. 3(b) breaks down the TMD losses: skin friction and mixing/recirculation account for most of the compressor loss, while rotor-passage loss dominates the turbine loss. These detailed efficiencies, which differ from the values assumed in the initial CCD, are fed back into the cycle model in Section 2.4.

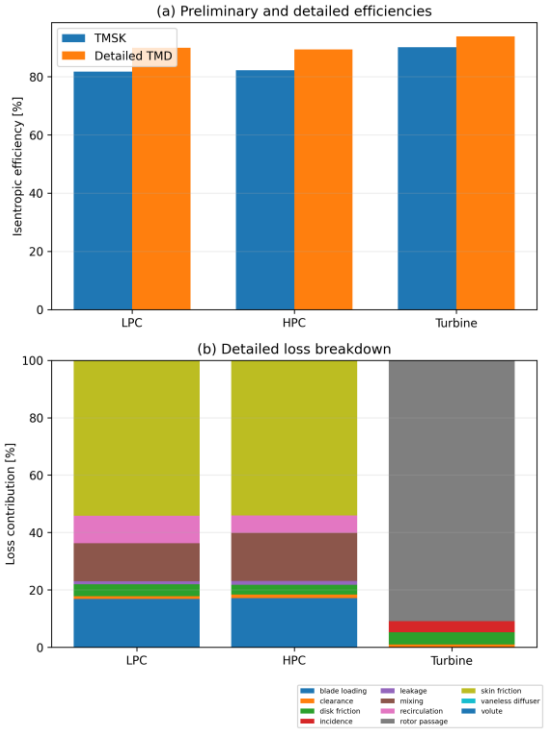


Fig. 3. Turbomachinery design results: (a) comparison of efficiencies predicted by preliminary TMSK and detailed TMD and (b) loss contributions for the detailed turbomachinery design

The rotor tip speed is obtained directly from the Euler turbomachinery work equation, solving for the blade speed that produces the stage's required stagnation enthalpy rise through a slip factor — Wiesner's for the compressor impeller and Stanitz's for the turbine rotor — and the rotor diameter is then derived from this tip speed and the fixed shaft speed. The characteristic diameter reported above is a different, larger diameter: the diffuser exits for the compressors and the nozzle or rotor inlet for the turbine, which are stationary components not subject to the tip-speed constraint.

2.4 TMD-informed Cycle Re-optimization

The detailed TMD analysis gave an LP compressor isentropic efficiency of 89.94%, an HP compressor isentropic efficiency of 89.38%, and a turbine isentropic efficiency of 93.86%. These values replaced the initial CCD assumptions, and the total pressure ratio and LP/HP split were re-swept with the reactor power, outlet temperature, minimum cycle temperature, recuperator effectiveness, and pressure drops all held unchanged from Section 2.1.

Table 2. CCD-only vs. TMD-informed optimum

Parameter	CCD-only	TMD-informed	Difference
LPC isentropic efficiency [%]	80.00	89.94	+9.94
HPC isentropic efficiency [%]	80.00	89.38	+9.38
Turbine isentropic efficiency [%]	88.00	93.86	+5.86
Total compressor PR [-]	1.869	1.993	+0.124
LP compressor PR [-]	1.342	1.393	+0.051
HP compressor PR [-]	1.398	1.436	+0.038
Helium mass flow [kg/s]	82.14	71.94	-10.20
Reactor inlet temperature [°C]	538.8	508.9	-29.9
Net power [MW]	35.67	43.45	+7.78
Thermal efficiency [%]	39.63	48.28	+8.65
Back-work ratio [-]	0.558	0.473	-0.085
Recuperator minimum ΔT [K]	23.6	22.1	-1.5

Fig. 4 compares the two cases. Fig. 4(a) shows thermal efficiency versus total pressure ratio for both: the TMD-informed curve lies uniformly above the CCD-only curve, and its optimum shifts from a pressure ratio of 1.869 to 1.993, with the thermal efficiency rising from 39.63% to 48.28%. Fig. 4(b) compares net power, mass flow, and back-work ratio at the two optima: net power rises from 35.67 to 43.45 MW, the required mass flow falls from 82.14 to 71.94 kg/s, and the back-work ratio drops from 0.558 to 0.473.

Table 2 helps explain why the mass flow falls: the reactor inlet temperature, state 8, drops from 538.8°C to 508.9°C between the two optima. Since the reactor duty is fixed at equation (6) and the reactor outlet enthalpy h1 is set by the fixed 750°C outlet temperature, a lower h8 widens the enthalpy rise across the reactor and allows the same 90 MW_{th} duty to be delivered with less mass flow. Because compressor power is large relative to turbine output in helium cycles, the higher TMD-derived efficiencies reduce compressor work, and as the cycle re-optimizes around this improvement, the pressure ratio that minimizes total compression work — not just the resulting efficiency — shifts together with the mass flow requirement. This shows that turbomachinery efficiency affects the optimal pressure ratio and mass flow, not only the efficiency magnitude, motivating a coupled cycle–turbomachinery design approach rather than one relying on fixed assumed efficiencies.

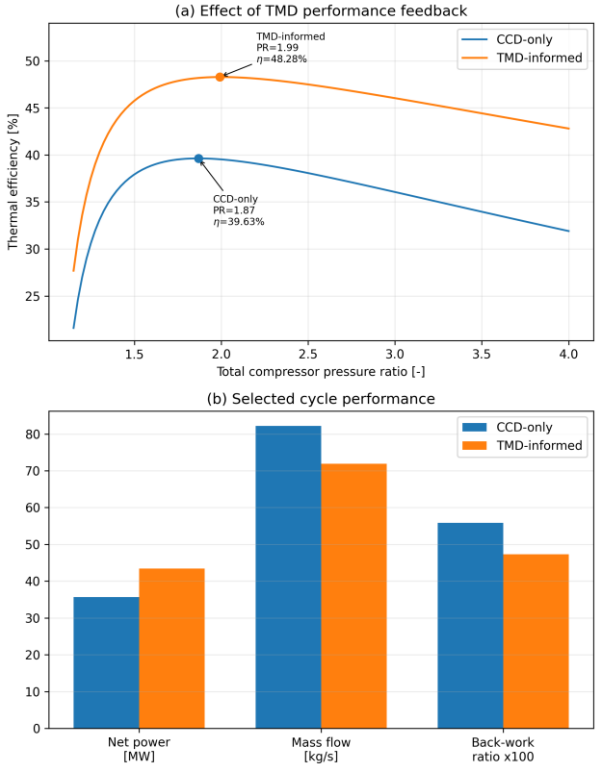


Fig. 4. Comparison of CCD-only and TMD-informed cycle optimization results

3. Results and Discussion

The CCD-only optimum (PR_{tot} = 1.869, η_{th} = 39.63%) showed a nearly equal LP/HP pressure-ratio split (1.342/1.398), with negligible efficiency difference between equal- and optimized-split cases — indicating total pressure ratio, not stage allocation, is the dominant lever on performance. The selected turbomachinery design, a radial configuration at 8,000 rpm with 2, 3, and 5 stages for the LP compressor, HP compressor, and turbine, gave detailed TMD efficiencies of 89.94%, 89.38%, and 93.86%, all exceeding the initial CCD assumptions. This gain came with constraints: characteristic diameters reached 1.54–1.77 m, and the turbine's tip speed reached 498.9 m/s, close to the 500 m/s limit — so higher achievable efficiency alone does not guarantee feasibility. Because these TMD

efficiencies come from the original CCD-only operating point rather than a TMD run at the re-optimized point, the following comparison is TMD-informed rather than fully coupled.

Feeding the TMD efficiencies back into CCD shifted the optimum from PR = 1.869 to 1.993, raised thermal efficiency from 39.63% to 48.28%, cut the required mass flow from 82.14 to 71.94 kg/s, and lowered the back-work ratio from 0.558 to 0.473, as summarized in Table 2. Since compressor power is large relative to turbine output in a helium Brayton cycle, the back-work ratio is dominated by the compressor side, and the compressor efficiency gain from 80% to roughly 90% alone is enough to shift the pressure ratio that minimizes compression work, not just the resulting efficiency, although Table 2 does not separately report turbine and compressor work. This shows that fixed-efficiency assumptions are adequate for conceptual screening, but detailed turbomachinery performance can shift both the optimal operating point and required mass flow, motivating coupled cycle-turbomachinery design for helium HTGR applications.

To test this, TMD was re-run at the TMD-informed optimum, where the total pressure ratio was 1.99 and the mass flow was 71.94 kg/s. The re-screened LP and HP compressors converged to feasible designs with efficiencies of 90.53% and 89.37%, respectively, but no feasible detailed turbine geometry could be found within the 500 m/s tip-speed limit. TMSK screening at this operating point selected a shaft speed of 9,000 rpm with 5 turbine stages, giving a screening-level tip speed of 470.8 m/s, yet every candidate detailed geometry exceeded the tip-speed constraint once the detailed loss model was applied. This is consistent with the baseline turbine design already operating close to the limit, since its tip speed of 498.9 m/s left only 1.1 m/s of margin, and it indicates that a fully coupled CCD/TMD iteration would require re-screening the turbine stage count and shaft speed, not just re-evaluating efficiency, at each step. Establishing such a fully coupled optimization, including stage-count re-screening, is left as future work.

4. Conclusions

This study coupled thermodynamic cycle optimization with turbomachinery design for a single-intercooled recuperated direct helium Brayton cycle applied to a 90 MW_{th} HTGR. The initial CCD analysis, using assumed efficiencies, gave a maximum thermal efficiency of 39.63% at PR_tot = 1.869, with a helium mass flow of 82.14 kg/s.

Turbomachinery design at this point selected a radial configuration at 8,000 rpm with 2, 3, and 5 stages for the LP compressor, HP compressor, and turbine. Detailed TMD analysis gave isentropic efficiencies of 89.94%, 89.38%, and 93.86% higher than the initial CCD assumptions — while the turbine's tip speed (498.9 m/s) approached the 500 m/s design limit.

Feeding these TMD efficiencies back into CCD shifted the optimum to PR = 1.993, raised thermal efficiency to 48.28%, reduced mass flow to 71.94 kg/s, and lowered the back-work ratio from 0.558 to 0.473. This shows that turbomachinery performance from detailed design, rather than fixed assumptions, meaningfully changes the optimal cycle design point.

Overall, this coupling shows that turbomachinery performance obtained from detailed design, rather than assumed values, can substantially shift the optimal cycle operating point, and that closing this loop further is limited by the turbine's tip-speed margin rather than by the optimization procedure itself.

REFERENCES

[1] Y. Ahn, J. Lee, and J. I. Lee, "Design of Helium Brayton Cycle for Small Modular High Temperature Gas cooled Reactor," *Transactions of the Korean Nuclear Society Spring Meeting*, Jeju, Korea, May 17-18, 2012.

[2] S. J. Bae, J. Lee, Y. Ahn, and J. I. Lee, "Preliminary Studies of Compact Brayton Cycle Performance for Small Modular High Temperature Gas-cooled Reactor System," *Annals of Nuclear Energy*, Vol. 75, pp. 11-19, 2015.

[3] C. B. Baxi, A. Shenoy, V. I. Kostin, N. G. Kodochigov, A. V. Vasyaev, S. E. Belov, and V. F. Golovko, "Evaluation of Alternate Power Conversion Unit Designs for the GT-MHR," *Nuclear Engineering and Design*, Vol. 238, pp. 2995-3001, 2008.

[4] C. F. McDonald, "Helium Turbomachinery Operating Experience from Gas Turbine Power Plants and Test Facilities," *Applied Thermal Engineering*, Vol. 44, pp. 108-142, 2012.

[5] L. Yao and Z. Zou, "A One-Dimensional Design Methodology for Supercritical Carbon Dioxide Brayton Cycles: Integration of Cycle Conceptual Design and Components Preliminary Design," *Applied Energy*, Vol. 276, 115354, 2020.

[6] E. W. Lemmon, I. H. Bell, M. L. Huber, and M. O. McLinden, "NIST Standard Reference Database 23: Reference Fluid Thermodynamic and Transport Properties—REFPROP, Version 10.0," National Institute of Standards and Technology, Gaithersburg, MD, 2018.

[7] O. E. Balje, *Turbomachines: A Guide to Design, Selection, and Theory*, Wiley-Interscience, New York, 1980.